Supporting Information

Exploring the phase behavior of C8-BTBT-C8 at ambient and high temperatures: insights and challenges from molecular dynamics simulations

Mosè Casalegno,*[,†] Simone Provenzano[‡], Guido Raos,[†] Massimo Moret,*[,§]

[†] Department of Chemistry, Materials and Chemical Engineering "G. Natta", Politecnico di Milano, via L. Mancinelli 7, 20131 Milano, Italy.

[‡]Applied Materials Inc., Reggio Emilia, Italy.

[§] Department of Materials Science, Università degli Studi di Milano-Bicocca, Via R. Cozzi 55, 20125 Milano, Italy.

Content:

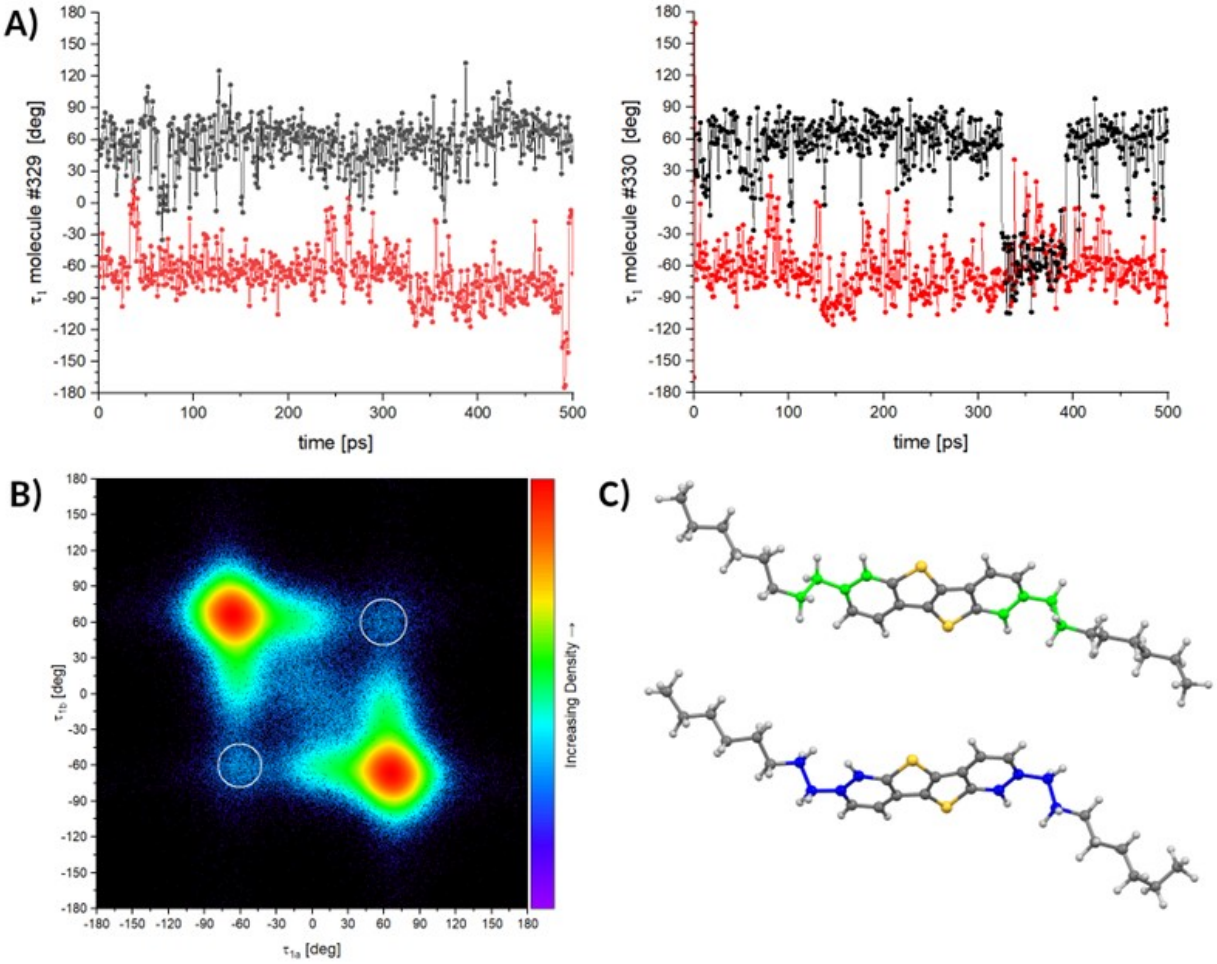

Figure S1. A) Trajectories of two randomly chosen molecules showing the dynamics of the alkyl chains. B) Density plot of torsion angle for chains A (τ_{1A}) and B (τ_{1B}). The white circles enclose the sparsely populated regions of torsions with the same sign. C) Two representative conformations with non-centrosymmetric chains (top, white circle region) and close to centrosymmetric (bottom, red region of the density plot).

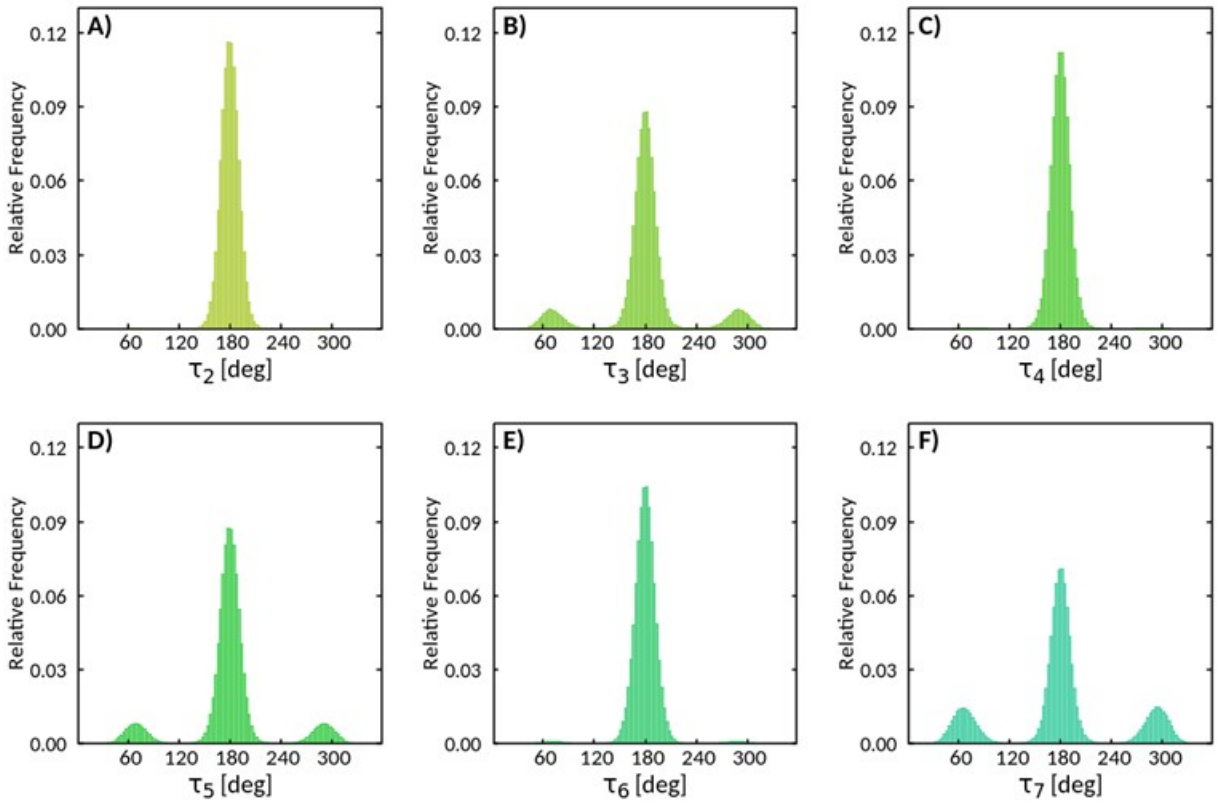

Figure S2. Probability distributions of angles τ_2-τ_7, characterizing the conformational behavior of the octyl chains at 293 K.

Table S1. Percentages of torsional angle conformations at 293 K, obtained from 500 ps of NPT-BE simulation. The signs + and – refer to τ around +67°, or around -67°, i.e. +293°, respectively.

Conformation	τ_2	τ_3	τ_4	τ_5	τ_6	τ_7
anti	99.70	83.31	99.20	81.84	97.66	65.77
gauche$^+$	0.14	8.42	0.44	9.03	1.15	17.15
gauche$^-$	0.15	8.26	0.36	9.14	1.19	17.08
gauche (total)	0.30	16.69	0.80	18.16	2.34	34.23

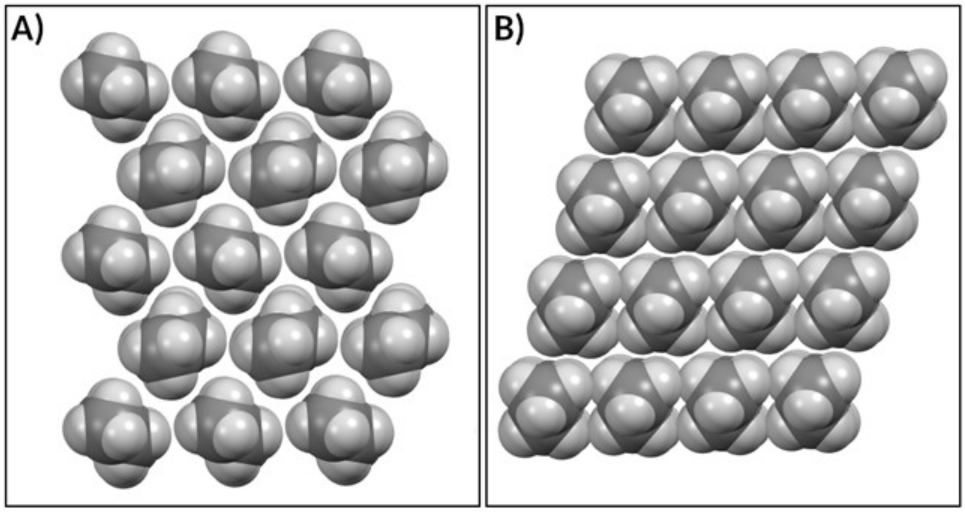

Figure S3. Views along the c axis of: A) C8-BTBT-C8 and B) octane monomolecular layers qualitatively comparing alkyl chain steric hindrance.

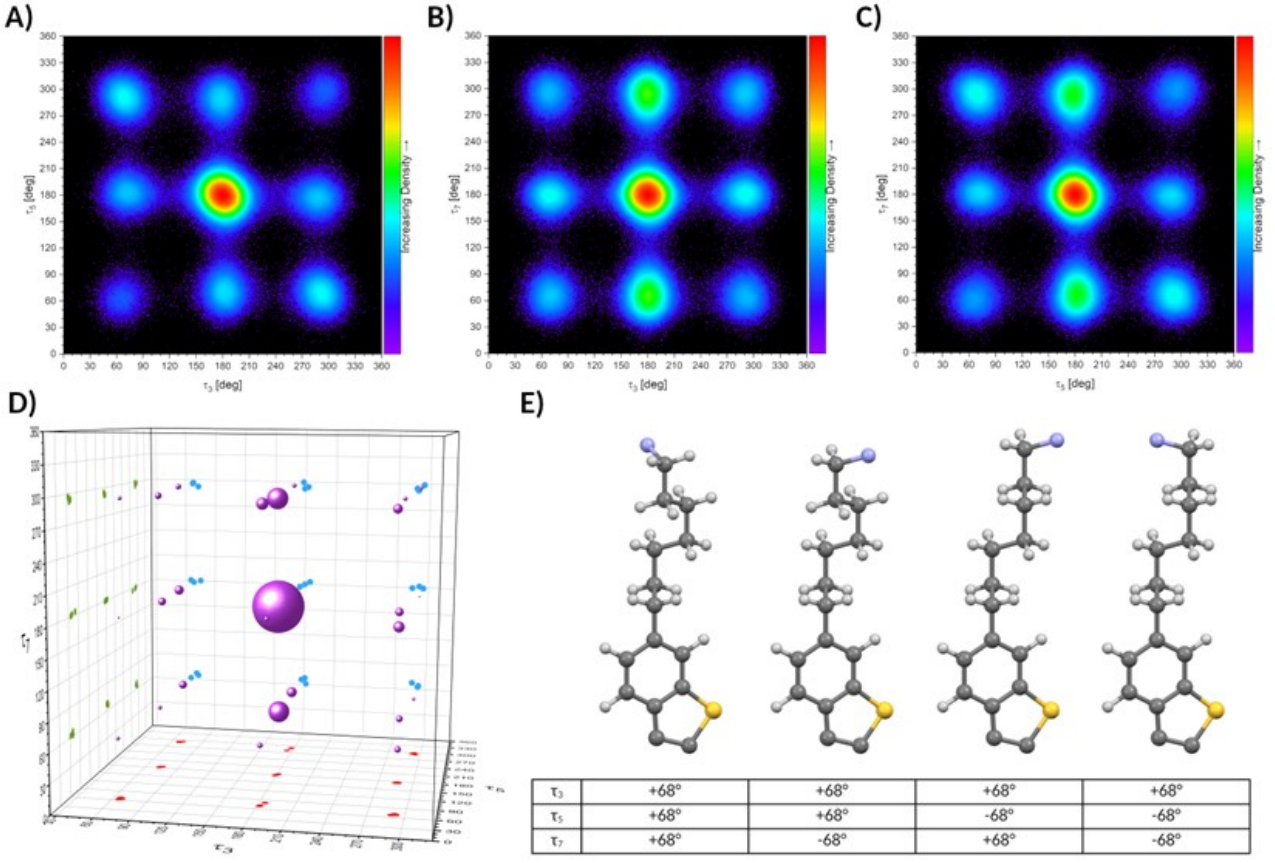

Figure S4. Distribution of torsion angles in subspace τ_3-τ_5-τ_7 showing the main conformational features of the octyl chains. A-C) Projections with density plots showing clustering of points; D) 3D plot showing data clustered in subspace τ_3-τ_5-τ_7; each sphere's size is proportional to the square root of the corresponding cluster size. E) Idealized *agagag* conformations observed in the 293 K MD run (four enantiomeric conformations of those shown here are also present). The methyl group carbon atom with hydrogen atoms omitted for clarity is highlighted in blue.

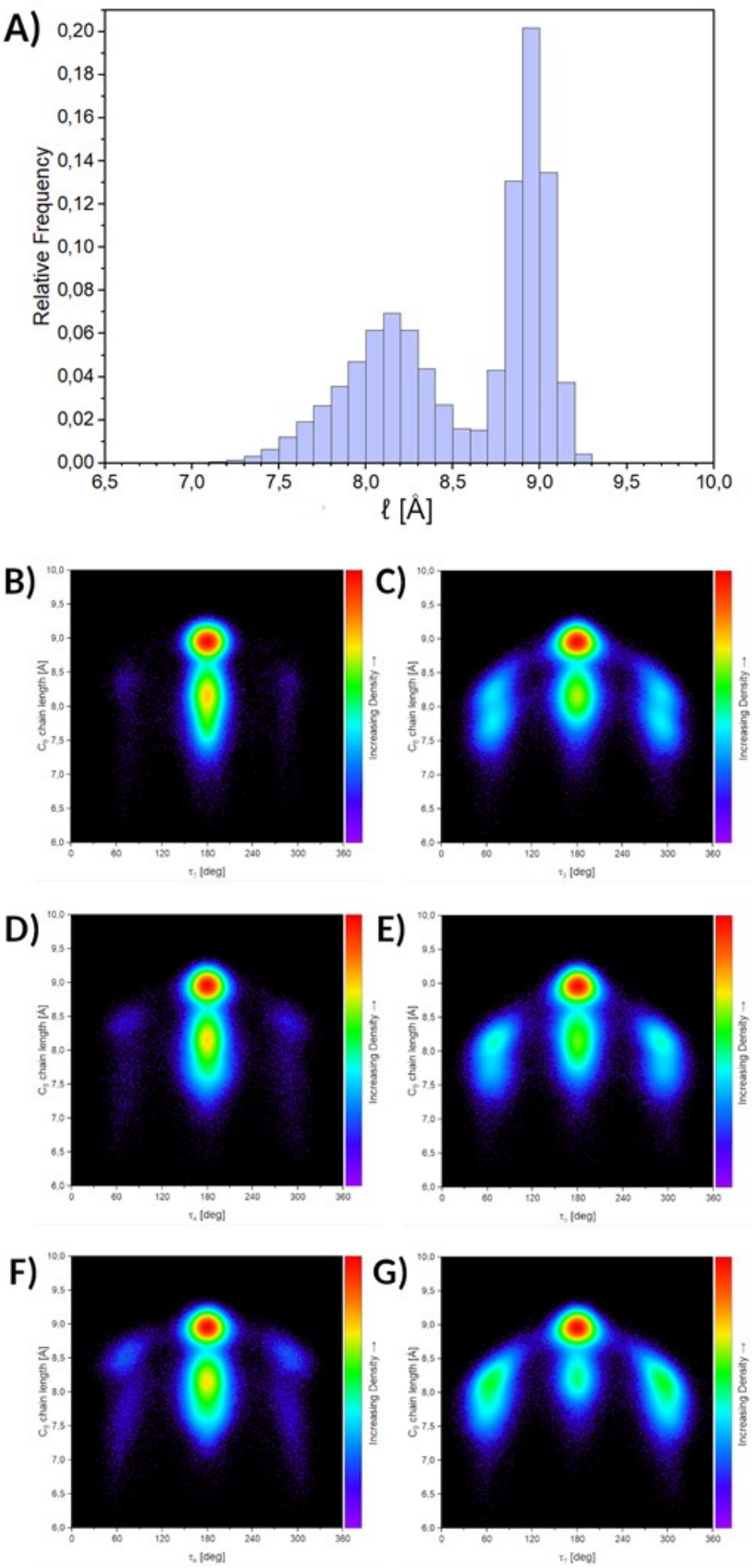

Figure S5. A) Probability distribution of alkyl chains length (ℓ). B-G) Density scatter plots of alkyl chain length versus torsion angles τ2-τ7.

Table S2. Percentages of *a* (*anti*) and *g* (*gauche*) torsional angle combined conformations at 293 K.

descriptor $\tau_2\tau_3\tau_4\tau_5\tau_6\tau_7$	% of cases
aaaaaa	55.59
aaaaag	18.44
aaagag	6.24
agagag	6.10
agagaa	4.50
agaaag	2.82
agaaaa	2.77
aaaaga	1.19
all	97.65

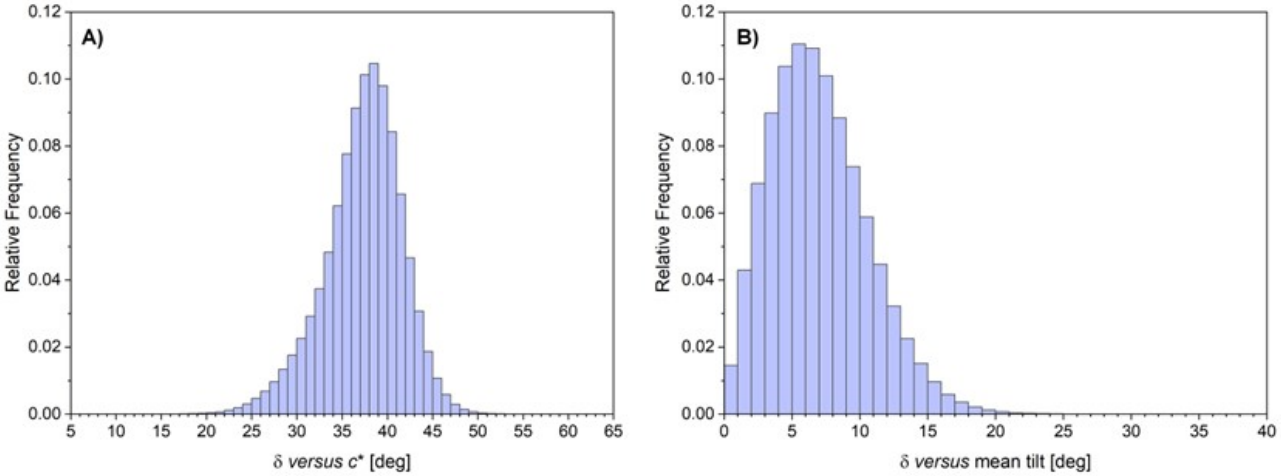

Figure S6. Distribution of chain tilt angle δ: A) versus direction c* and B) versus mean tilt direction for chains A and B merged due to centro-symmetry of the system.

Table S3. Average values of the tilt angle δ from the 500-ps NPT-PR simulation at 293 K. Standard deviations are given in parentheses.

reference	δ [deg]
c* axis	37.3(4.3)
mean tilt	7.02(3.6)

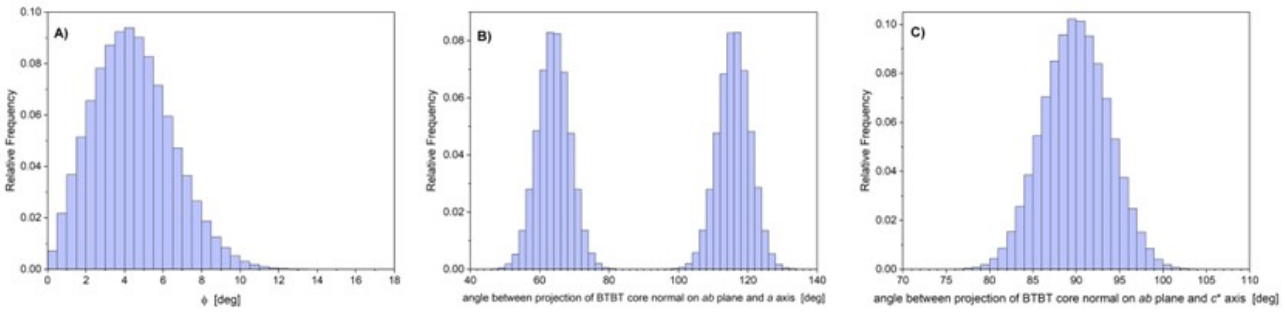

Figure S7. Distribution of A) the core tilt angle φ. B) The angle between the projection onto the *ab* plane of the normal to the BTBT core and *a* axis. C) The angle of the BTBT core normal with respect to the reciprocal vector *c**.

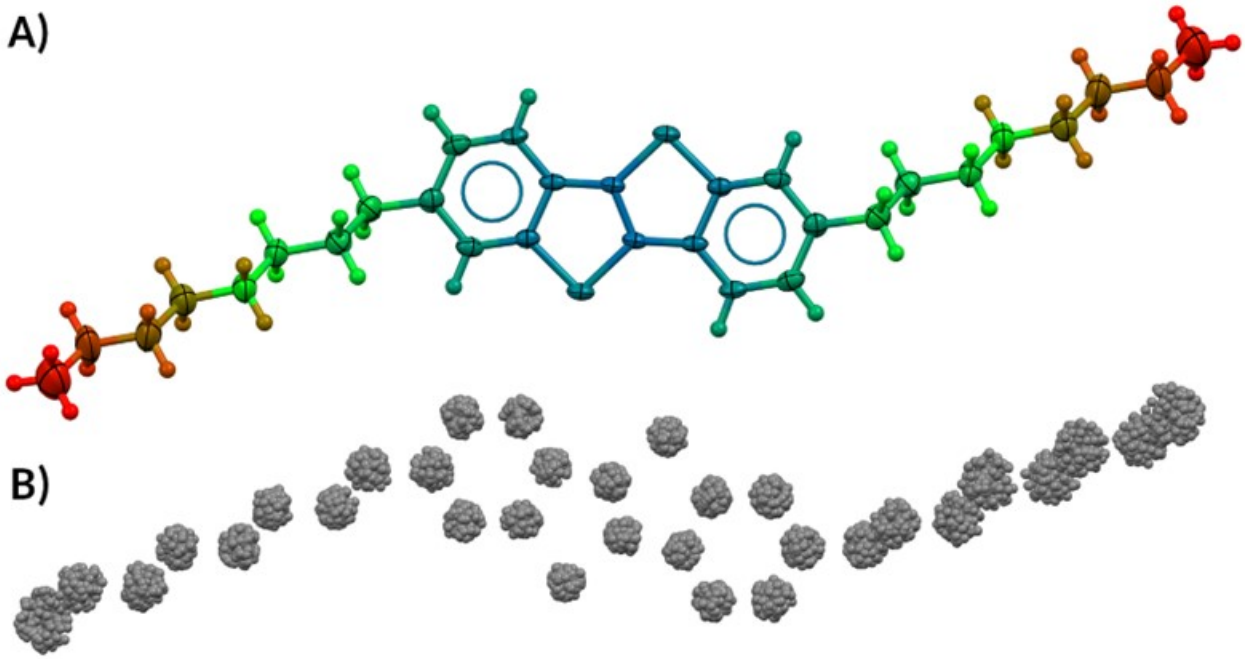

Figure S8. A) Molecular structure of C8-BTBT-C8 in the monoclinic polymorph [Izawa, T. et al. *Adv. Mater.* 2008, 20 (18), 3388–3392]. Non hydrogen atoms are represented with 30% level ellipsoids enhanced with fake colors (from blue to red for low to high ADP values). B) Non-hydrogen atomic positions for molecule #300 in the 293 K MD run; grey spheres correspond to the closest 30% of atomic positions with respect to their pertinent time averaged C and S atoms.

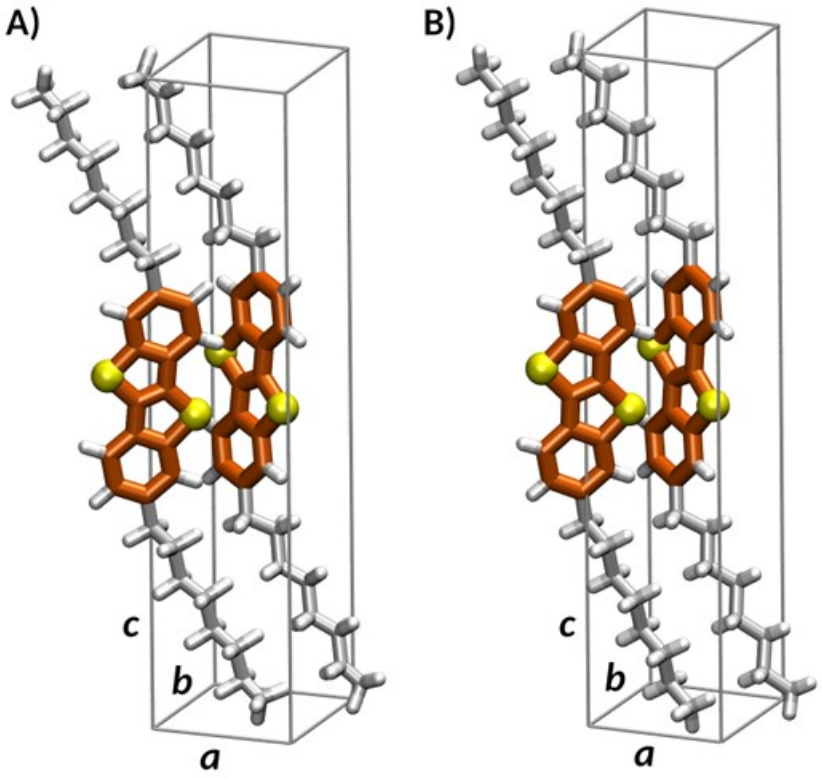

Figure S9. C8-BTBT-C8 unit cells: A) Average MD crystal structure obtained from the NPT-PR simulation at 293 K by averaging the atomic coordinates over 500 ps, whilst keeping two independent molecules. B) Experimental structure at 293 K [Izawa, T. et al. *Adv. Mater.* 2008, 20 (18), 3388–3392].

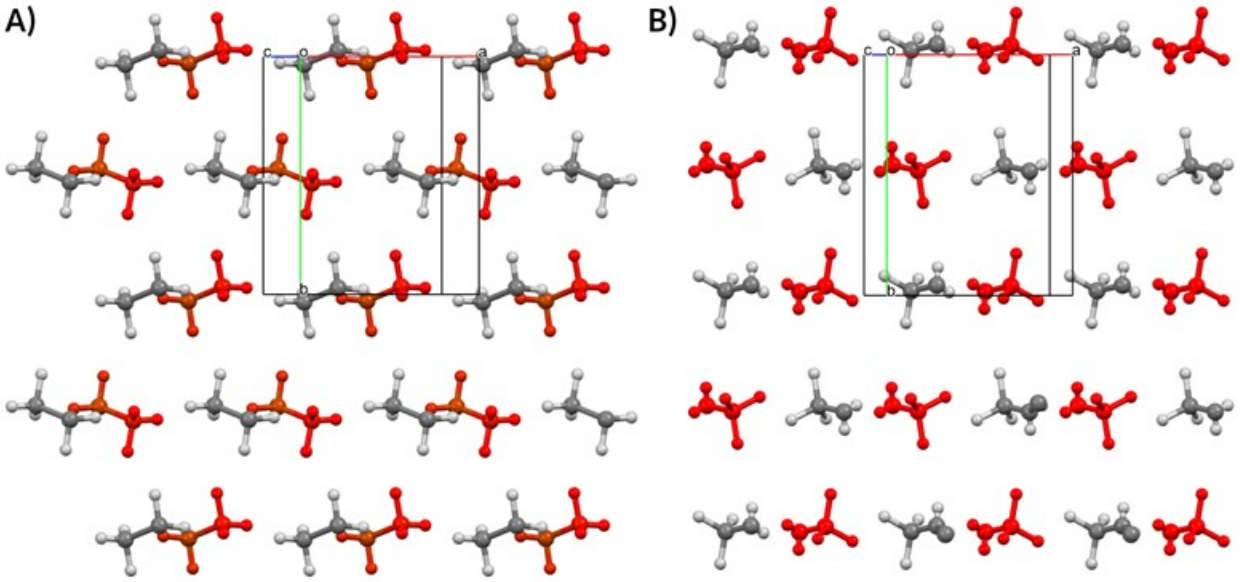

Figure S10. Comparison of two adjacent (001) monomolecular layers as seen along *c** enhancing the differences between A) the experimental [Izawa, T. et al. *Adv. Mater.* 2008, 20 (18), 3388–3392] and B) the average MD crystal structure.

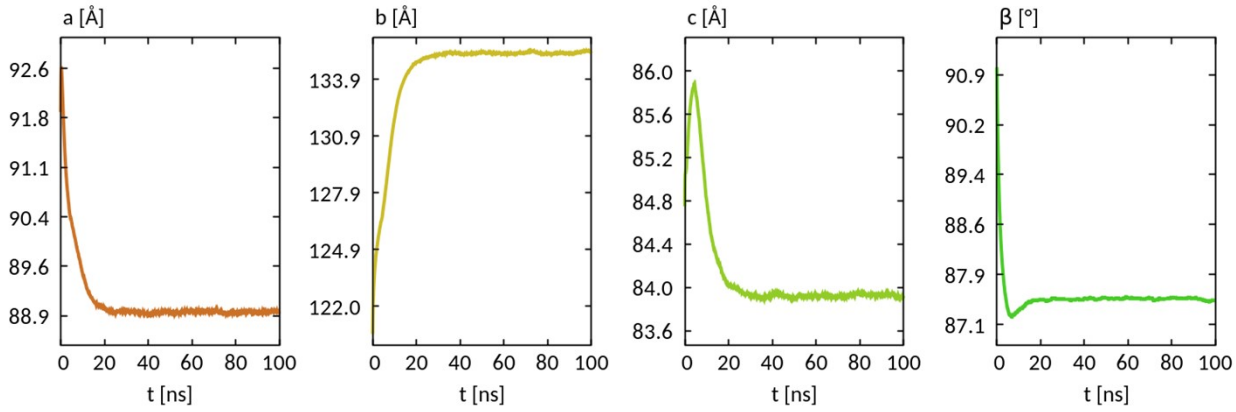

Figure S11. Evolution of simulation box parameters at 380 K.

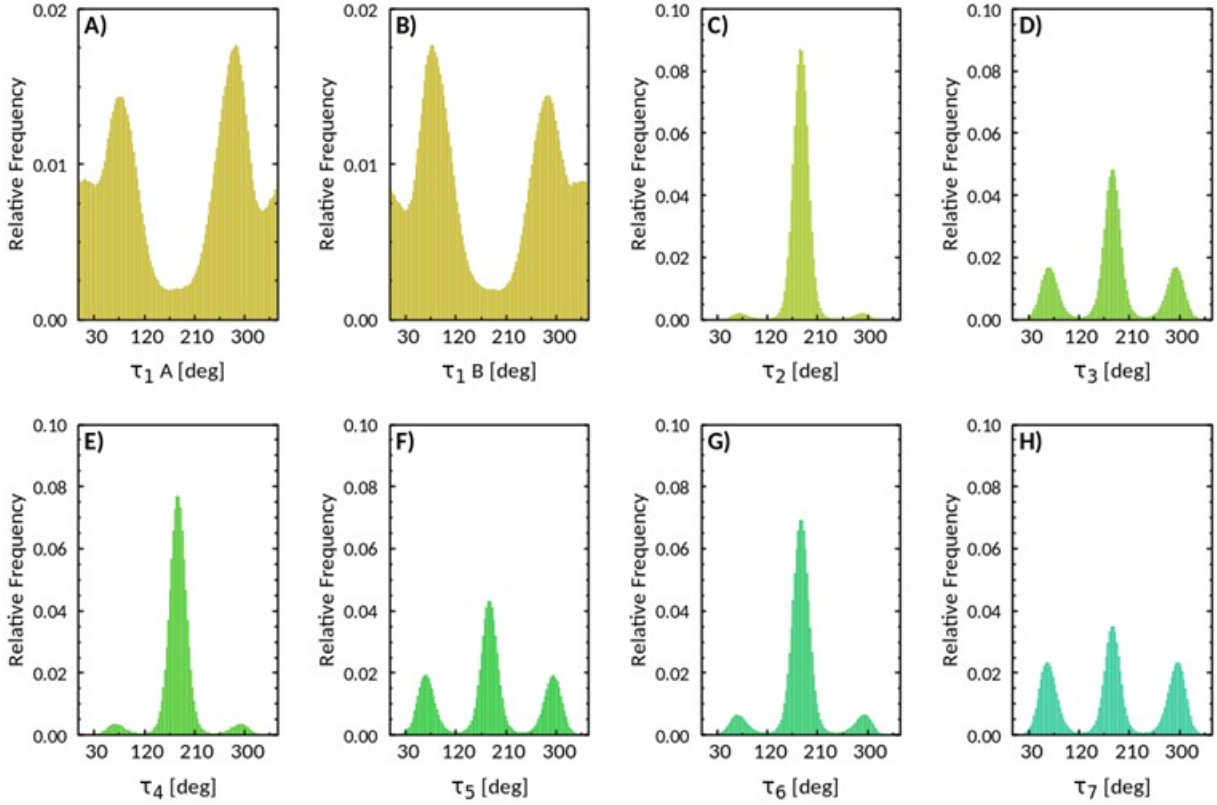

Figure S12. Cumulative dihedral angles distributions obtained from the NPT-BE run at 380 K.

Table S4. Percentages of *a* (anti) and *g* (gauche) torsional angle combined conformations at 380 K. Only those exceeding 1% of cases are reported.

descriptor $\tau_2\tau_3\tau_4\tau_5\tau_6\tau_7$	**% of cases**
aaaaag	15.73
agagag	14.14
aaagag	12.37
aaaaaa	10.96
agagaa	8.20
agaaag	7.80
aaagaa	5.45
agaaaa	4.53
aaaaga	2.64
aaaagg	1.95
agagga	1.46
aaaggg	1.25
aaagga	1.14
agaggg	1.06
aagaga	1.04
all	89.72

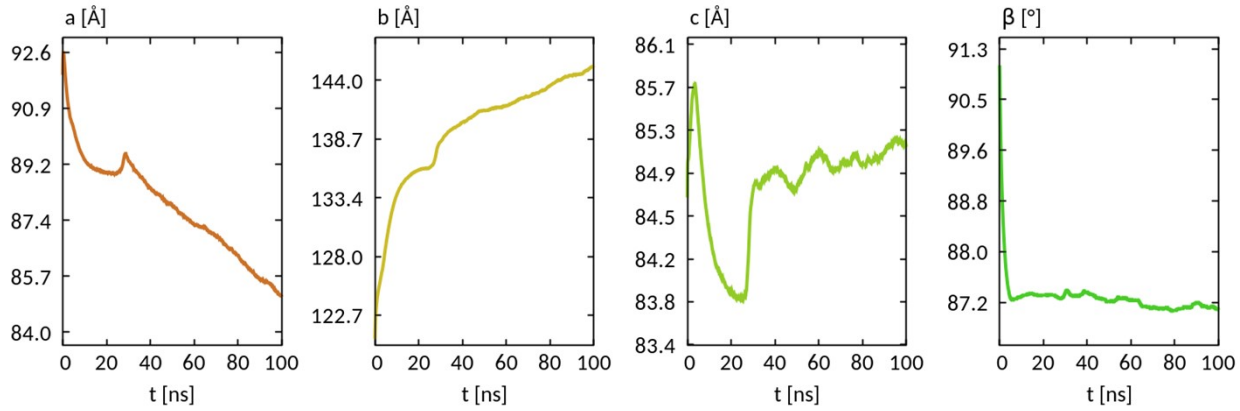

Figure S13. Evolution of simulation box parameters at 385 K.

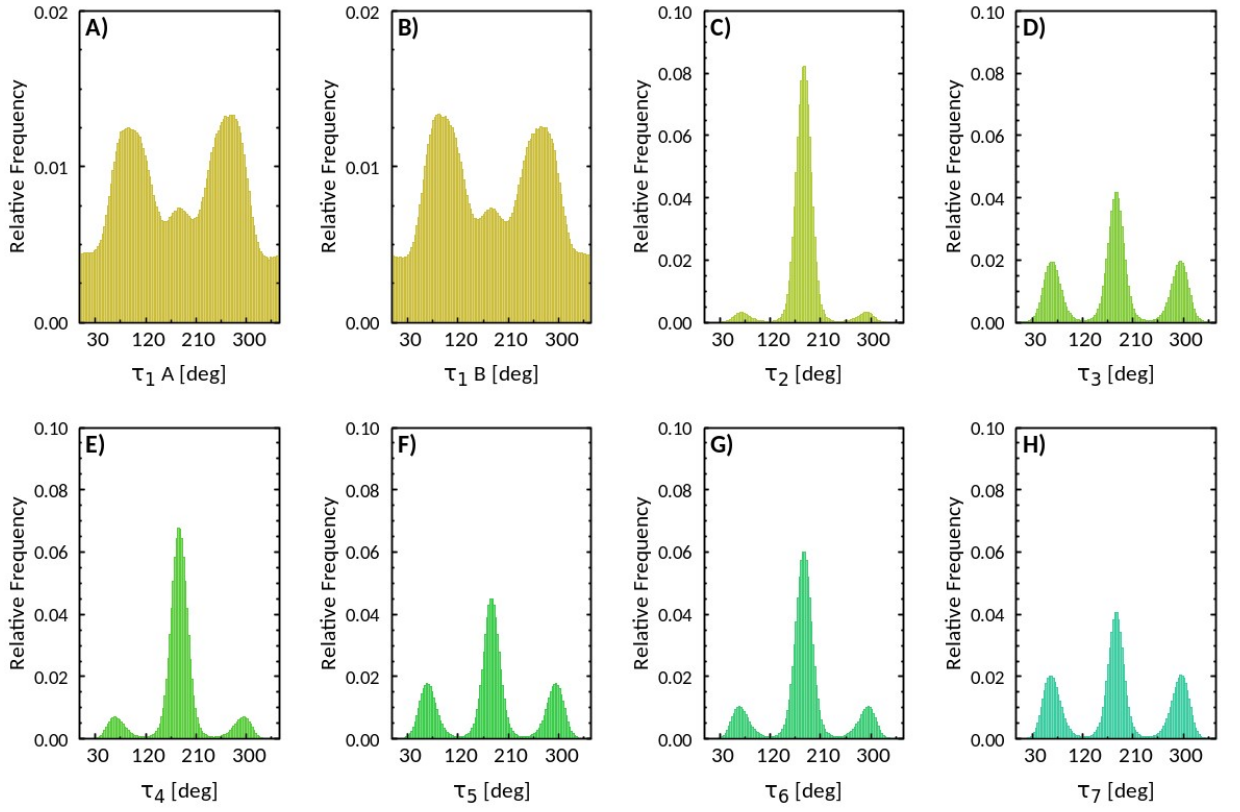

Figure S14. Cumulative dihedral angles distributions obtained from the NPT-BE run at 385 K.

Table S5. Percentages of *a* (anti) and *g* (gauche) torsional angle combined conformations at 385 K. Only those exceeding 2% of cases are reported.

descriptor $\tau_2\tau_3\tau_4\tau_5\tau_6\tau_7$	**% of cases**
agagag	11.11
aaaaag	8.24
aaaaaa	7.51
aaagag	7.24
agagaa	7.16
agaaag	7.10
agaaaa	5.67
aaagaa	4.27
aaaaga	3.09
agaaga	2.66
agagga	2.29
aaaagg	2.00
all	68.34

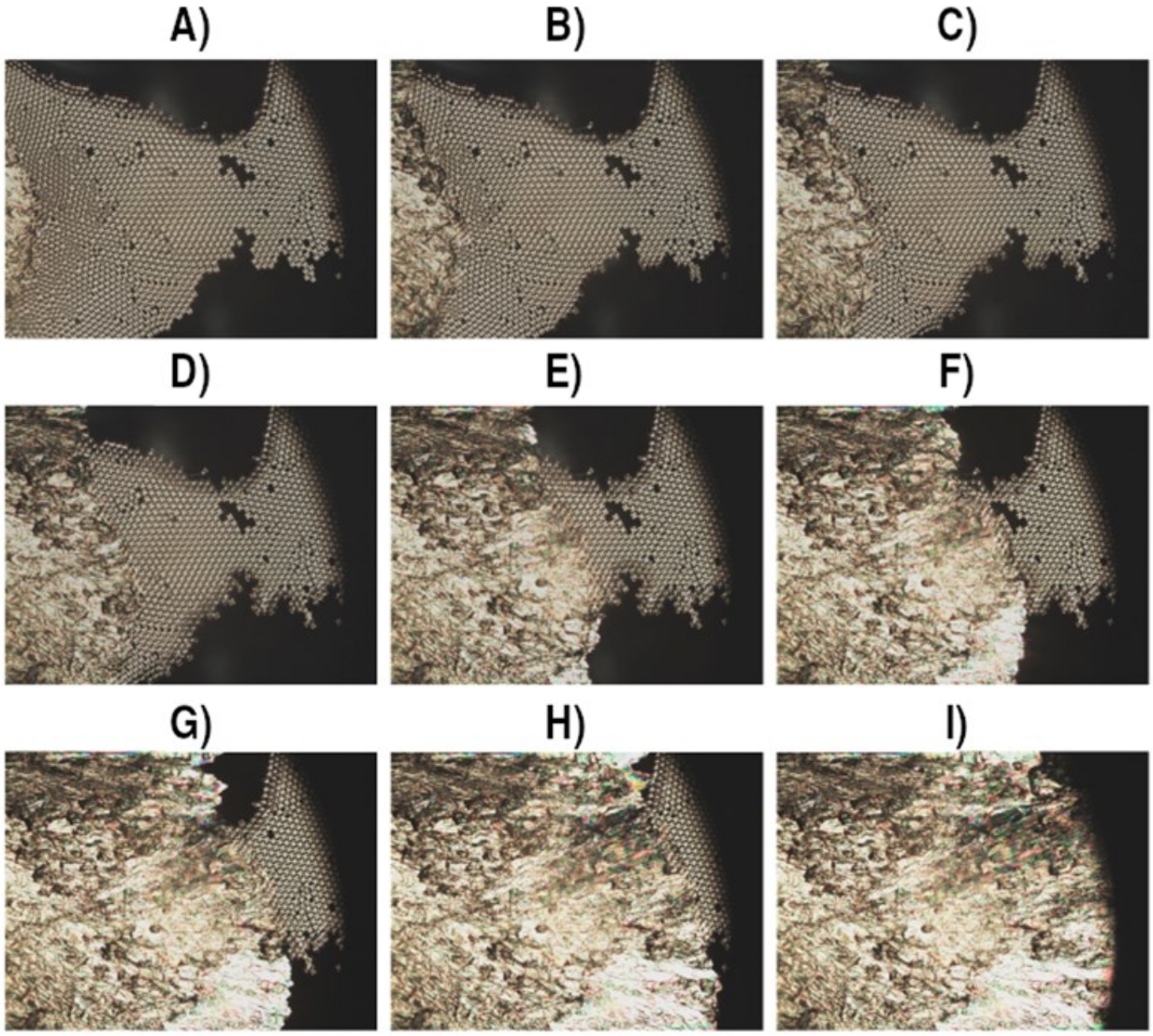

Figure S15. Focal conic domains (FCD) of the mesophase during cooling. The sequence was taken at 377 K (104 °C). The (micro)crystalline phase appears on the left of the imaged region. Images taken with Linkam THMS-600 heating stage (sample loaded in an open quartz cup) and metallographic microscope Olympus BX51 at 50x (images 1440 μm along the horizontal axis) with crossed polarizer/analyzer.

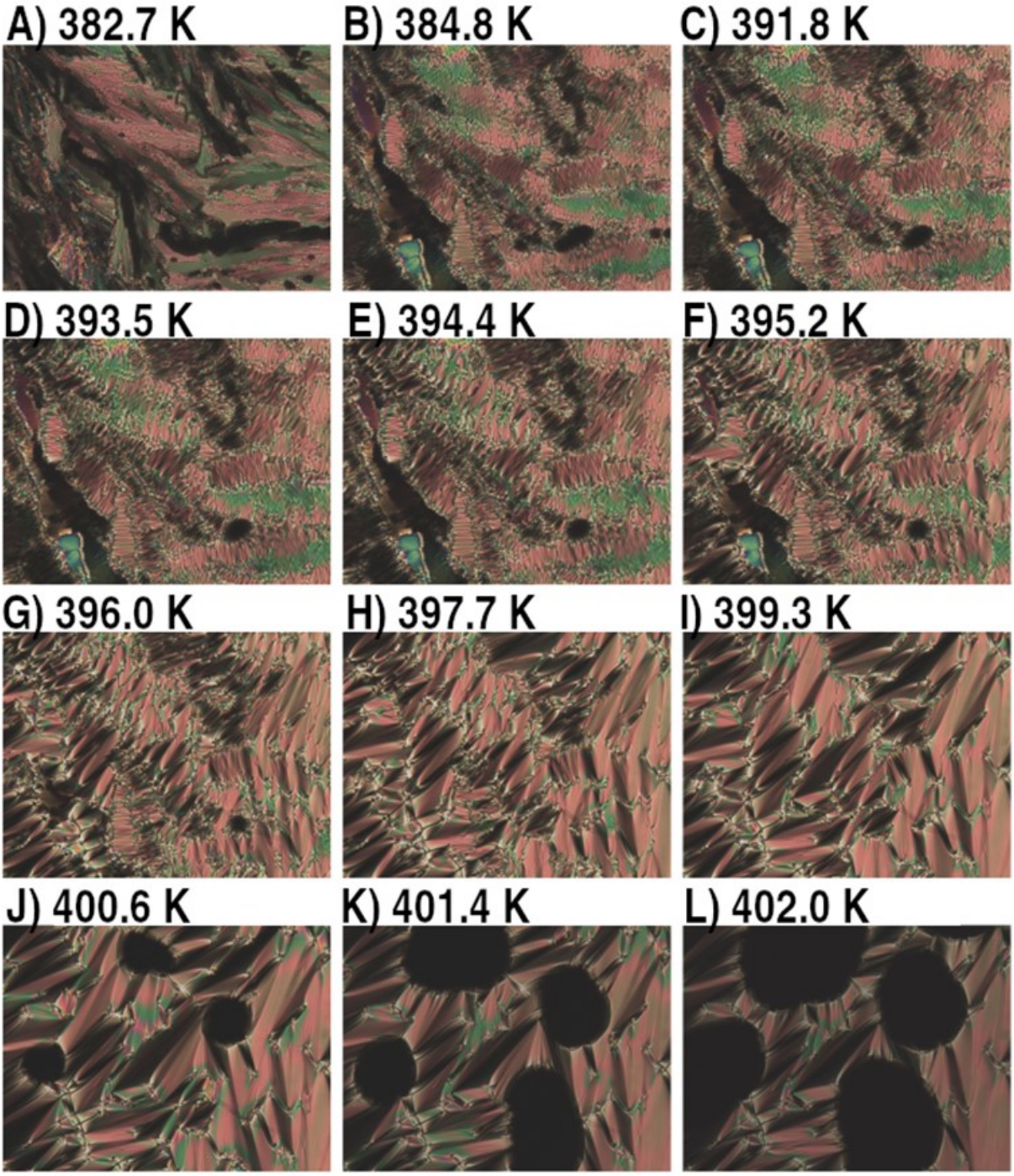

Figure S16. Smectic A large domains rearrange upon heating (heating rate +1 K/min) producing small striped domains (B-D) further coarsening into fan-shaped big islands (E-I) and eventually melting (J-L). The dark regions in images J-L correspond to expanding regions of isotropic melt. Images taken with Linkam THMS-600 heating stage (sample loaded in an open quartz cup) and metallographic microscope Olympus BX51 at 200x (images 360 μm along the horizontal axis) with crossed polarizer/analyzer. Nominal temperatures reported suffered from thermal gradients in the central hole drilled out in the silver block of the heating stage.

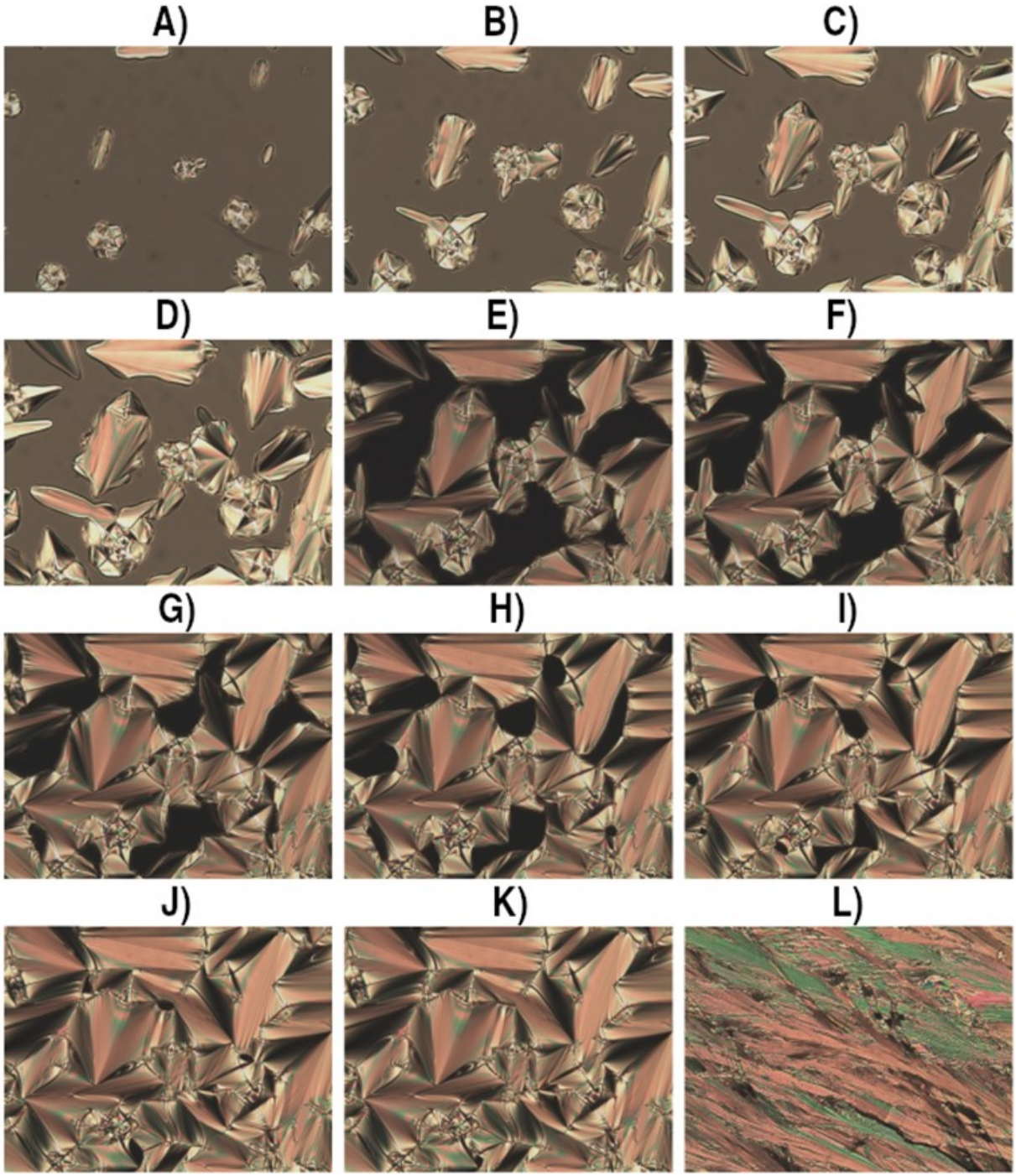

Figure S17. Starting from the isotropic liquid (before frame A) and cooling at -1 K/min fan-shaped domains of the mesophase are formed (A-K) that eventually give rise to the crystalline state (L). Images taken with Linkam THMS-600 heating stage (sample between a quartz cup and 0.16 mm thick coverslip) and metallographic microscope Olympus BX51 at 50x (images 1440 μm along the horizontal axis) with parallel (images A-D) and crossed (E-L) polarizer/analyzer.

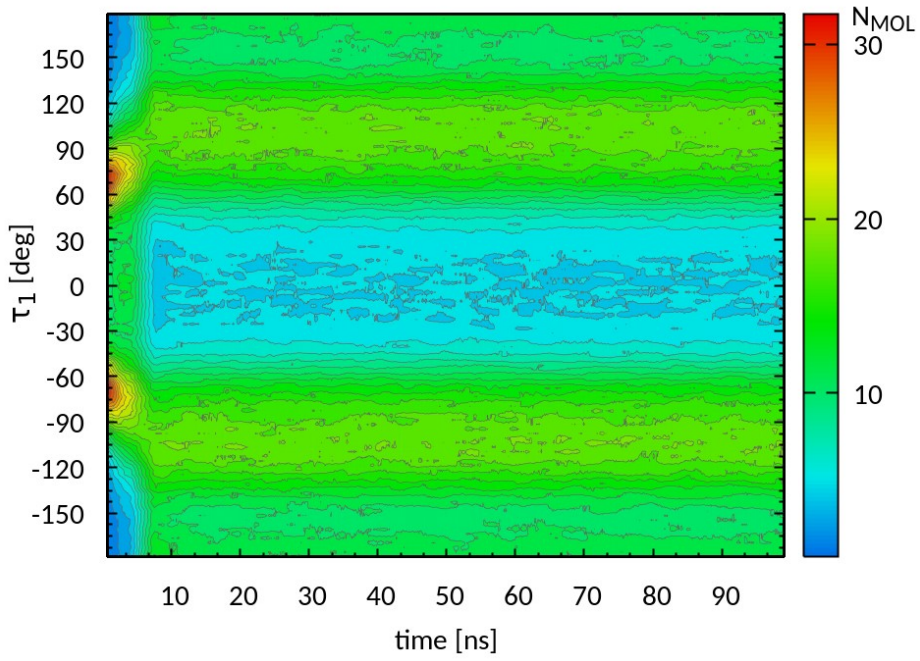

Figure S18. Evolution of the tilt angle φ obtained from the NPT-BE simulation at 400 K. The absolute molecular populations are also reported. For better clarity, the data have been window-averaged over time intervals of 3 ns.

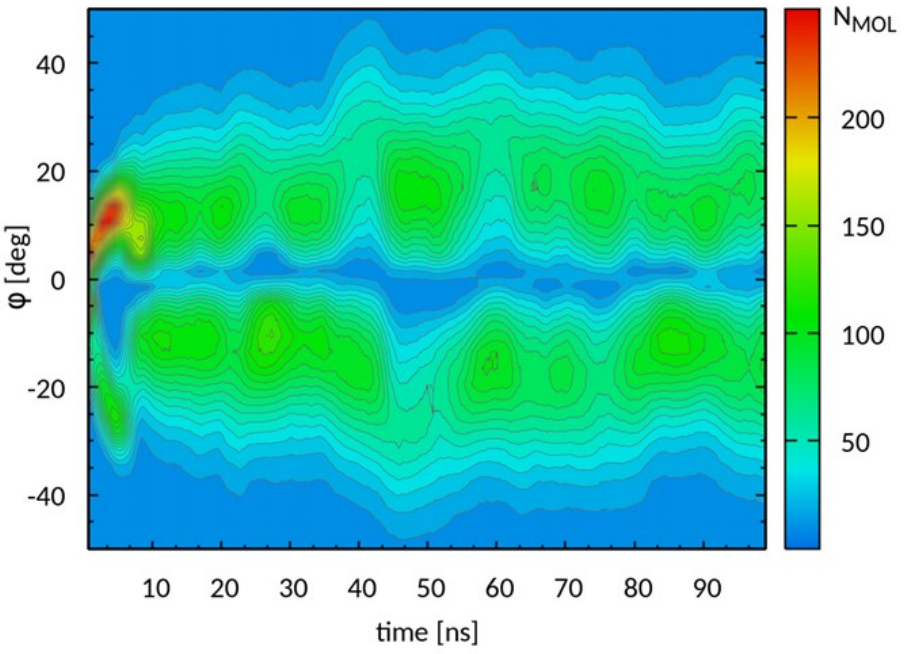

Figure S19. Evolution of the torsional angle τ_1 obtained from NPT-BE simulations at 400 K. The absolute molecular populations are also reported. For better clarity, the data have been window-averaged over time intervals of 3 ns.

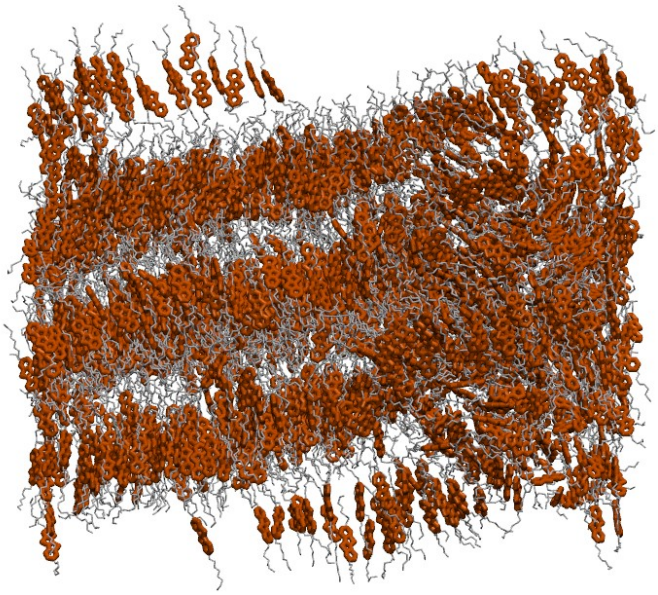

Figure S20. Final snapshot of the 100-ns BE simulation performed by cooling the isotropic molten phase from 460 to 385 K. A linear temperature gradient was adopted over a simulation time of 100 ns.

Movie S1. Dynamics of C8-BTBT-C8 supercell at 385 K, highlighting the change in core tilt angle, φ, and diffusion phenomena. The molecules have been colored according to their orientation (red for $\varphi < 0°$, blue for $\varphi > 0°$). Alkyl side chains and hydrogens have been omitted for clarity.